The microbial adhesive arsenal deciphered by atomic force microscopy

Audrey Beaussart, Cécile Feuillie, Sofiane El-Kirat-Chatel

The microbial adhesive arsenal deciphered by atomic force microscopy

Audrey Beaussart[1], Cécile Feuillie[2], Sofiane El-Kirat-Chatel[3]*

[1]Université de Lorraine, CNRS, LIEC, F-54000 Nancy, France

[2]CBMN, CNRS UMR 5248, IPB, Université de Bordeaux, 33607 Pessac, France

[3]Université de Lorraine, CNRS, LCPME, F-54000 Nancy, France

*Corresponding author:

Sofiane El-Kirat-Chatel: elkirat1@univ-lorraine.fr

GRAPHICAL ABSTRACT

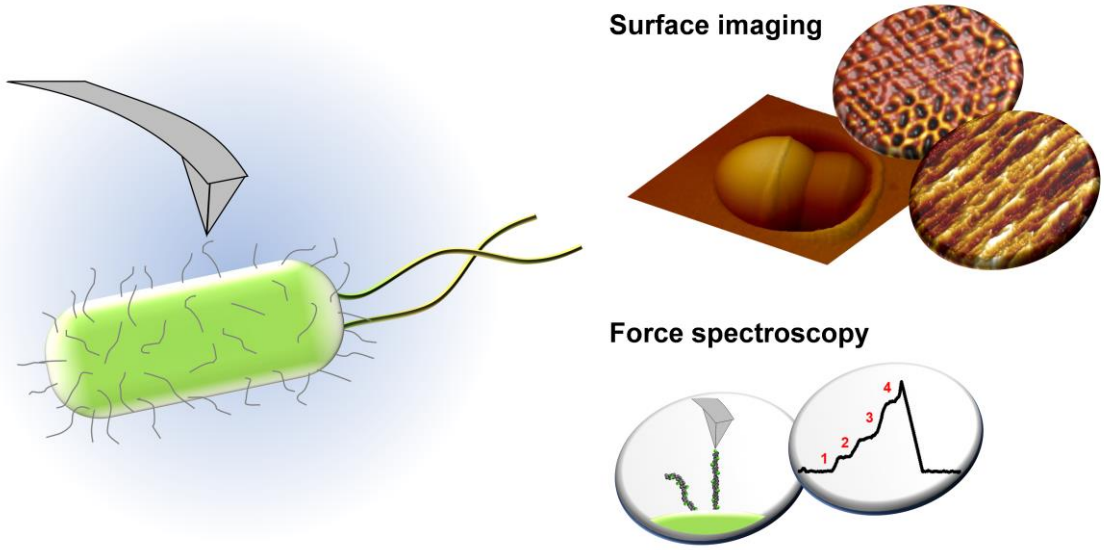

ABSTRACT

Microbes employ a variety of strategies to adhere to abiotic and biotic surfaces, as well as host cells. In addition to their surface physicochemical properties (*e.g.* charge, hydrophobic balance), microbes produce appendages (*e.g.* pili, fimbriae, flagella) and express adhesion proteins embedded in the cell wall or cell membrane, with adhesive domains targeting specific ligands or chemical properties. Atomic force microscopy (AFM) is perfectly suited to deciphering the adhesive properties of microbial cells. Notably, AFM imaging has revealed the cell wall topographical organization of live cells at unprecedented resolution, and AFM has a dual capability to probe adhesion at the single-cell and single-molecule levels. AFM is thus a powerful tool for unravelling the molecular mechanisms of microbial adhesion at scales ranging from individual molecular interactions to the behaviours of entire cells. In this review, we cover some of the major breakthroughs facilitated by AFM in deciphering the microbial adhesive arsenal, including the exciting development of anti-adhesive strategies.

The microbial adhesive arsenal deciphered by atomic force microscopy

Introduction

Microorganisms commonly live in biofilms,[1,2] *i.e.* cell communities embedded in self-produced extracellular polymeric substances (EPSs) and adhered on substrates.[2] In this organization, some features typical of microorganisms emerge, such as quorum sensing, resistance or tolerance to antimicrobials, and cell differentiation. This successful life style has thus allowed the ubiquitous presence of microorganisms on Earth: they are associated with biogeochemical cycles, biotechnological processes, and life-threatening infections in plants and animals.[1,2]

Biofilm formation begins with the initial attachment of microbial cells to biotic or abiotic substrates.[3] This adhesion is mediated by properties of the cell surface, *i.e.* the cell wall, the ultimate interface between a cell and its environment, and which gives the cell its shape and protects it from external stresses.[4,5] Bacteria are the microbial kingdom dominantly involved in biofilms, followed by fungal cells, and are classified into two groups according to their cell-wall organization: Gram-positive bacteria have cell walls containing a thick peptidoglycan layer covered by anionic acids such as (lipo)teichoic acids, whereas the cell walls of Gram-negative bacteria present a thinner peptidoglycan layer coated by an outer membrane comprising phospholipids and lipopolysaccharides. Fungal cell walls comprise an inner layer containing chitin and β-glucans and an outermost layer composed of mannoproteins.

Whatever the genus, microorganisms have evolved a plethora of adhesive strategies to colonize diverse environments. The major effectors for cell adhesion are: i) the physicochemical properties of the cell surface (*e.g.* charge, hydrophobic balance) and ii)

appendages (including pili, fimbriae, flagella) and the expression of adhesins, polymers embedded in the cell wall or cell membrane that present domains adhering to specific ligands or chemical properties. Although this adhesive arsenal has been progressively highlighted since the early 1950s through microscopy, molecular biology, and biochemistry, its role in microbial adhesion was often only hypothesized or indirectly demonstrated by empirical methods comparing wild types and mutant strains.

Since its invention in 1986 by Binnig *et al*., atomic force microscopy (AFM) has emerged as a powerful tool for probing the properties of microbial surfaces at high resolution while the cell remains alive.[6] The principle of AFM is to scan a sample surface with a sharp tip (radius of few nanometers) mounted on a flexible cantilever. While scanning, interactions between the tip and the surface bend the cantilever, and this deflection is monitored using a laser beam focused at the apex of the cantilever and reflected into a multi-segment photodiode. The precise positioning of the sample during scanning is controlled by a piezoelectric scanner moving in x, y and z directions. Because the tip physically touches the sample, AFM can image sample topography at sub-nanometer resolution and sense interaction forces on the order of a few piconewtons. The recently developed force-distance-based multiparametric imaging mode has allowed the imaging of biological structures while simultaneously quantifying and mapping their physical, chemical, and/or biological properties.[7-9] In addition to imaging, microbiological prospects have largely benefited from the advances in AFM-based force spectroscopy methodologies, and more particularly from the development of the single-molecule (SMFS) and single-cell force spectroscopy (SCFS) techniques, where the apex of the tip is decorated by a single biomolecule or a single microorganism, respectively.

In this review, we report some of the major breakthroughs in our understanding of microbial cell surface organization facilitated by AFM.

Microbial cell surfaces at the nanoscale

Cell wall organization and ultrastructure.

In the last two decades, AFM has provided remarkable insights into the cell wall architecture of microbes. AFM is advantageous compared to other high-resolution techniques (*e.g.* electron microscopy, crystallography) because it can be performed in liquid to analyse samples in physiologically relevant conditions. Yet, AFM microbe analyses require cell immobilization, *i.e.* attaching the microbes on a solid substrate to allow the cell surface to be scanned without lateral displacement. As microbial cells are often round and negatively charged, most immobilization methods rely on electrostatic interactions[10-12] or mechanical trapping in pores.[13-15] Each immobilization technique can induce a bias and should be carefully chosen according to the cell properties to be measured. For instance, cell trapping in porous membrane is very relevant to study cell biomolecules unfolding, as no chemicals are involved, preventing unwanted interactions with the AFM tips. However, the physical constraint applied on the cell might influences its nanomechanical properties. Others anchoring methodologies such as support-coating by chemicals (*e.g.* gelatine, polyethyleneimine, poly-lysine) should be privileged in this case.

For Gram-positive bacteria, the thick layer of peptidoglycan largely contributes to the cell-wall rigidity and is the most-exposed structure underneath the polysaccharidic surface layer. On the other hand, the thin layer of peptidoglycan in Gram-negative bacteria is overlaid by a soft and unstable outer lipid membrane. Therefore, immobilisation methods, imaging and

force measurements are usually straightforward for Gram-positive bacteria, while their application to Gram-negative bacteria is often more delicate.

Using the approaches mentioned above, different bacteria have been imaged at high resolution, revealing diverse cell surface features. The presence of proteinaceous surface layers (S-layers) give *Viridibacillus arvi*, *Lysinibacillus sphaericus*, and *Corynebacterium glutamicum* textured surfaces with repeated motifs (Fig. 1).[16,17] Single-cell imaging of *Lactobacillus rhamnosus* and *Lactobacillus plantarum* revealed rough surfaces attributed to adhesive extracellular polysaccharides and teichoic acids, respectively.[18,19] As peptidoglycan is a major building block of all bacterial cell walls, major efforts have also been made to decipher its organisation. However, until recently, its three-dimensional arrangement remained controversial. AFM imaging has solved this issue for *Lactococcus lactis* mutant devoid of cell wall polysaccharides, as topographic images revealed 25-nm-wide periodic ridges running parallel to the cell short axis. Chemical identification was verified by force spectroscopy using LysM-decorated tips. These results confirmed observations previously made on purified *Bacillus subtilis* sacculi (exoskeletons).[20,21] Li *et al.* showed that peptidoglycan organization is more variable than previously thought and changes during cell growth (Fig. 1A),[22] consistent with observations of *Streptococcus* and *Escherichia coli* (Fig. 1B).[23,24] Nanoscale multiparametric imaging of polysaccharide intercellular adhesin (PIA)-expressing *Staphylococcus aureus* cells showed the presence of a soft and adhesive extracellular matrix surrounding the cells.[25]

Given its capability to image cell topographies at unprecedented resolution, several groups have used AFM to study cell wall changes during cell division, exposure to external stresses (*e.g.* drugs), etc. Eskandarian *et al.* showed that mycobacterial division occurs within a hollow between two crests on the undulating cell surface, which they linked to the

underlying peptidoglycan organization.[26] Similarly, time-series analyses showed that *Staphylococcus aureus* cells present a hairy surface during the exponential phase and progressively bald during the stationary phase.[27] AFM has also helped decipher the main steps of bacterial infection by phages. Protruding phages were detected at the surfaces of *E. coli*, *Salmonella enteritidis*, and *Bacillus thuringiensis*.[28-30] Using multiparametric AFM, Alsteens *et al.* showed that phages are extruded from densely packed areas corresponding to soft nanodomains in the cell septum.[29] Surface changes can also occur when cells are exposed to drugs. The digestion of *S. aureus* cell walls by lysostaphin was directly observed on live cells by time-resolved imaging.[31] Similarly, Formosa *et al.* revealed that antibiotics affect cell roughness and remove the caspule of *Pseudomonas aeruginosa* and *Klebsiella pneumonia*, respectively.[32,33]

Yeasts cells have been also investigated by AFM imaging. For instance, AFM analyses of *Saccharomyces cerevisiae*, *Saccharomyces carlsbergensis*, *Candida glabrata*, and *Candida albicans* have revealed smooth surfaces that can present bud scars.[34-37] Most fungi undergo morphogenesis, during which they grow into elongate cells that are difficult to immobilize, hindering their analysis by AFM. Yet, Beaussart *et al.* immobilized *C. albicans* germ tubes on hydrophobic surfaces to image and probe the major cell wall components involved during pathogenesis.[38] El-Kirat-Chatel *et al.* used correlative AFM-fluorescence imaging to decipher the main steps of *Candida*-macrophage interaction: after 3 h, the macrophage membrane is pierced by long germ tubes formed by internalized yeasts, on which pieces of the macrophage are leftover.[39]

AFM can also be used to explore changes in bacteria and yeast cells induced by physical or chemical treatments such as antibiotics. Heat treatment induces the formation of large circular structures on *S. cerevisiae*,[40] and antifungal treatments have led to abnormally shaped

yeasts.[41-44] In particular, caspofungin, an antifungal drug that blocks the synthesis of β-1,3-glucans, increases the cell surface roughness and adhesiveness of *C. albicans*.[42,43]

Bacterial appendages.

Besides its basal composition, the bacterial cell wall is often decorated with protruding proteinaceous structures, *e.g.* flagella and pili, that are involved in motility, adhesion, cell-cell transfer, and pathogenesis.[3] Such appendages are typically imaged in air as they are too labile/flexible to be imaged in liquid. Curved structures longer than bacterial cell bodies and corresponding to flagella have been detected in images of *Pseudomonas fluorescens*, *Bacillus thuringiensis*, and *E. coli*,[45-48] and smaller, rod-shaped appendages corresponding to pili or fimbriae have been detected in images of *Lactobacillus rhamnosus*, *P. aeruginosa*, *Corynebacterium diphtheria*, *E. coli*, and *Salmonella*.[46,49-53] Flagella are always longer and larger than pili and fimbriae. Imaging these structures in physiologically relevant conditions remains challenging, though we anticipate that the development of new multiparametric AFM modes will contribute to the acquisition of topographical data on the appendages on living microbes.

Detect, pull, unfold: the molecular biophysics of microbial surface-associated biomolecules

Biofilm formation depends on the successful adhesion of pioneer cells.[2] Consequently, microbes have evolved a large arsenal of adhesive mechanisms to stick to substrates and withstand mechanical shear. Understanding these molecular adhesion mechanisms is key to developing new antibiofilm strategies and may also inspire new biotechnological concepts.

Force spectroscopy has revolutionized our understanding of the microbial surface characteristics. In details, the AFM tip is successively approached and pulled away from the cell surface, resulting in a so-called force-distance curve. During the approach phase, the force acting on tip starts to increase directly after the contact between the tip and the biosurface is established. The tip can then be considered as a 'nanoindentor' that allows to sense the nanomechanics of the microbial surface. In the retract phase, the tip pulling on the surface biomolecules results in their unfolding. The retract curve can be composed of a single peak or a succession of peaks corresponding to the unfolding of the different domains forming the molecules. The shape of this unfolding curve is related to the nature of the biomolecules (*e.g.* protein, polysaccharide) and to its structure (*e.g*. the presence of repeated domains, the number of amino-acids in each domains). In SMFS, specific molecular probes are attached to the AFM tips, which allows mapping and unfolding of adhesive molecules expressed at microbial cell surfaces. Single-molecule stretching depends on the mechanical response of biomolecules when subjected to external forces, which can be directly linked to their cellular function.

To adhere to their support, bacteria need to withstand mechanical perturbations such as host coughing, sneezing or liquid flow. Bacterial adherence is usually maintained by extracellular protein appendages called pili. Using specific probes, the mechanical responses of pili under external applied force have been deciphered by SMFS. For instance, pulling individual pili from the Gram-positive bacteria *Lactobacillus rhamnosus* resulted in stepped force-distance curves presenting peculiar linear increases and horizontal plateaus, suggesting that these appendages behave like nanosprings under force stimulation (Fig. 2 A-C).[54-56] In these studies, pili were pulled with tips bearing pilin subunits or milk proteins, further illustrating their dual involvement in homotypic interactions with and adhesion to dairy components. The

pathogenic Gram-positive bacteria *Streptococcus pyogenes* and *Streptococcus pneumoniae* produce adhesive pili to colonize host surfaces. Unfolding of *S. pyogenes* pili by SMFS indicated that the major pilin is an inextensible protein, and that this peculiar mechanical resilience is attributed to isopeptide bonds strategically located in the pili structure.[57] Further analysis of the adhesive properties of *S. pyogenes* pili revealed that the reactivity of the pili adhesins -containing thioester functions- with their ligands is mediated by mechanical force. Indeed, the adhesion is governed by the pili adhesins folding state, which controls whether the thioester bond could be cleaved or not.[58] Pili of Gram-positive bacteria are also capable to dissipate energy through mechanical unfolding and refolding of polypeptides loops contained in the pili structures. Such an example are the CnaA loops in the pili of *Corynebacterium diphtheriae* and *Actinomyces oris,* which are highly stable and resist pulling forces of up to 500 pN, acting to dissipate mechanical energy and help bacteria resist shear forces.[59] SMFS also allowed to reveal that another Gram-positive bacteria, *S. pneumoniae*, expresses pili that contain two regions binding simultaneously to host fibronectin, and that this mechanism favours an efficient scan of the colonized surface, targeting specific cells for interaction and invasion.[60] The same group has also demonstrated that the backbone protein of this pilus binds to collagen I in a force-dependent manner, resembling the so-called catch-bond mechanism.[61]

In contrast, the unfolding of the pili and fimbriae of Gram-negative bacteria reveal completely different force signatures. Pulling on type-1 fimbriae from *E. coli* with mannose-decorated tips produced force curves with constant force plateaus and long rupture distances (up to 10 µm),[62] attributed to the uncoiling of the quaternary structure of fimbriae during the catch-bond interaction with mannose residues, an interaction that is strengthened under tensile mechanical force. The specific interaction between mannose and *E. coli* fimbriae was demonstrated by using mannosylated tips to probe wild-type and mutant cells devoid of

appendages.[63] This study demonstrated a possible antiadhesive property of mannosylated fullerenes, which can simultaneously interact with and block multiple fimbriae.[63] Interestingly, the different Fim domains of *E. coli* fimbriae are organized in a hierarchical mechanical architecture; domains close to the outer membrane present higher mechanical stability than those exposed at the apex of the appendage.[64] On *P. aeruginosa*, hydrophobic tips were used to probe type-IV pili, producing force plateaus similar to those observed for *E. coli* pili.[49] By comparing different mutant strains, these authors concluded that the pili structure governed this hydrophobic interaction.[49]

In addition to appendages, bacterial adhesion can also be promoted by adhesins, *i.e.* adhesive proteins anchored at the cell surface. As for pili, SMFS with tips bearing specific probes can be used to map the distribution and probe the mechanics of individual adhesins at the surfaces of living cells. Using heparin tips, single heparin-binding hemagglutinin adhesins were detected on the surface of *Mycrobacterium bovis* and were found to be grouped in nanodomains.[65] Filamentous hemagglutinin adhesins at the surface of *Bordetella pertussis* were detected with antibody-bearing tips, which revealed a force-induced reorganization of adhesins on the cell surface to reinforce bacterial attachment under external forcing.[66] The specific force signature resulting from molecular unfolding during SMFS also gives crucial information on the mechanical properties of adhesins. In *Pseudomonas fluorescens*, adhesion is finely controlled by the Lap regulation system in which LapA is the surface exposed adhesin.[67] This protein is known to promote adhesion to surfaces of various physicochemical properties and contains a cell wall-anchoring domain, 37 repeated sequences, and a C-terminal globular domain (Fig. 2D). The mechanical response of LapA has been deciphered by SMFS with tips decorated with specific antibodies (Fig. 2E). Unfolding LapA led to force signatures presenting regular sawtooth patterns that were attributed to the successive

unfolding of the 37 repeats (Fig. 2F).[68] High environmental inorganic phosphate concentrations induce the exposure of LapA to promote cell adhesion, whereas decreased concentrations lead to the cleavage of LapA to allow cells to explore other environments.[69] Substrate-adhered LapA presents multiple adhesive peaks with no regular shape, reflecting that LapA interacts via multiple substrate domains. Moreover, the LapA distribution on the substrate corresponds to areas where bacteria had previously adhered, indicating that LapA is left on the substrate as bacterial 'footprints'.[70]

SMFS was also used to decipher the nanobiophysics of *Staphylococcal* adhesion, especially for the two major pathogens *Staphylococcus epidermidis* and *Staphylococcus aureus*. During infection, *Staphylococci* express different adhesins grouped as microbial surface components recognizing adhesive matrix molecules (MSCRAMMs) to bind to their host surfaces.[71] To characterize the contribution of SdrF adhesins in the adhesion of *S. epidermidis* to collagen, recombinant *Lactococcus lactis* expressing the *S. epidermidis* SdrF gene was probed with collagen-decorated tips.[72] This revealed that regions A and B of SdrF form strong and weak bonds with collagen, respectively, and both interactions present high dissociation rates.[72] *L. lactis* also served to demonstrate the specific recognition of fibrinogen by SdrG.[73] On *S. epidermidis*, probing SdrG with fibrinogen tips resulted in a remarkably strong interaction of ~2 nN;[72,74] such strong forces were previously only reported for covalent bonds.[75] Although the fibrinogen-SdrG interaction withstands high forces, it does not correlate with high affinity (K_d ≈ 400 nM).[76] This high mechanical stability is thus attributed to the N2 and N3 domains of SdrG, which operate the so-called "dock, lock, and latch" (DLL) mechanism on the target and allow strong mechanical attachment.[76] Further SMFS analysis coupled with all-atom steered molecular dynamics (SMD) simulations confirmed this high interaction force

and identified that a minimal six-residue sequence in the fibrinogen is sufficient for SdrG DLL binding.[77]

Similarly high interaction forces (~1.5 nN) were reported for the collagen-binding protein Cna of *S. aureus* using collagen tips.[78] In this case, SMFS was used to decipher the nanospring role of the CnaB region in the collagen hug mechanism, whereas the A region is involved in initial ligand binding and can be blocked by monoclonal antibodies. The capability of Cna to bind to other host proteins was also established with tips decorated with laminine or the complement system protein C1q.[79] This study demonstrated that Cna is a multifunctional adhesin that can bind several host proteins through different mechanisms to increase the probability of *S. aureus* adhesion. In the dual binding modes of the *S. aureus* clumping factors A and B (ClfA and ClfB) to the fibrinogen and loricrin proteins of the host, respectively, mechanical tension can convert an initial weak interaction into a strong one involving a DLL mechanism with N2N3 subdomains.[80,81] The dual binding mode of ClfA to fibrinogen was further confirmed by injecting blocking agents *in situ* during AFM experiments: only strong interactions were blocked by a short Fg γ-chain peptide.[80] Strong adhesion was also reported between *S. aureus* protein A and the plasma glycoprotein vonWillebrand factor. Analyses of this interaction in flow chambers revealed that strong interactions are induced by high shear forces.[82] Furthermore, the DLL conformation of *S. aureus* fibronectin-binding proteins (FnBPs) adopted when bonded to fibrinogen dramatically increases the plasminogen interaction.[83] Similarly, the interaction of FnBPA with host integrins is strongly enhanced in the presence of fibrinogen, forming a triple interaction involving FnBPA, the host fibrinogen, and $\alpha 5\beta 1$ integrin.[84] These results have revealed the cryptic role of FnBPs and showed that bacterial adhesins have evolved towards multipotent effectors for successful cell adhesion.

297 During infection, biofilm formation requires not only adhesion to host surfaces, but
298 also cohesion between neighbouring bacteria. In *S. aureus*, this second function has been
299 highlighted for FnBPA and SdrC cell wall proteins.[85,86] In both cases, the interaction involves
300 homophilic bonds between proteins of two adjacent cells.

301 SMFS has also revealed the molecular mechanisms governing the surface properties
302 of fungal cells. Probing the mechanical response of individual WSC1 proteins at the surface of
303 *Saccharomyces cerevisiae* revealed that this protein behaves like a nanospring, acting as a
304 mechanical force sensor by forming force-induced clusters on the yeast surface.[87] Exploiting
305 this typical mechanical response, the authors used truncated and elongated versions of WSC1
306 to demonstrate that the yeast cell wall is ~200 nm thick.[88] In the fungal pathogen *Candida*
307 *albicans,* cell adhesion is governed by proteins of the Agglutinin-like sequence (Als) family.[89]
308 These proteins share a common structure with an immunoglobulin (Ig)-like region, followed
309 by an amyloid-forming region, a tandem repeat (TR) region, and a stalk region anchored in the
310 cell wall. SMFS was used to unravel the mechanisms by which Als proteins promote yeast
311 adhesion. The unfolding of single Als proteins at the surfaces of living cells produced force
312 signatures presenting sawtooth patterns, in which each peak corresponded to the quantum
313 force required to unfold one repeat of the TR region.[90,91] Consecutive Als mapping on the same
314 cell resulted in the remarkable formation of adhesive patches, documenting the capacity of
315 Als to form clusters upon mechanical stimulation.[90] The role of Als in yeast cell adhesion was
316 also demonstrated during the cell stress response to caspofungin and during
317 morphogenesis.[38,42] The presence of Als in these conditions was correlated with increased cell
318 surface hydrophobicity by chemical force microscopy (CFM), where AFM tips are decorated
319 by methyl-terminated thiols to decipher the sample hydrophobicity with a few-nanometres
320 lateral resolution. This increased hydrophobicity was attributed to the exposure of TR domains

by unfolded Als proteins.[38,42,43] The amyloid-forming region was shown to be involved in homophilic zipper-like interactions and the formation of adhesive nanodomains.[92,93]

In *Candida glabrata*, the second major human fungal pathogen, Epa adhesins are known to bind to host cells through lectin-like interactions.[94] In addition, it was recently shown by CFM that Epa6 confers strong surface hydrophobicity to *C. glabrata* and may promote adhesion to abiotic surfaces.[37] In *S. cerevisiae*, analysis of the lectin function of Flo1 with a mannose-decorated tip revealed that Flo1 presents mechanical properties similar to Als in *C. albicans*, with a repeat region leading to sawtooth force-distance curves.[95]

As demonstrated above, the ultrasensitivity of AFM to force changes can be used to decipher adhesive mechanisms at molecular resolution. Another challenge is to understand how adhesive molecules work together at the scale of the entire cell, in both the contexts of cell-substrate and cell-cell interactions. To address single-cell adhesion, single-cell force spectroscopy (SCFS) was recently adapted to microbial cells.

SCFS methodologies to study microbial cells at the single-cell level

In SCFS, the AFM probe is decorated with a single cell and used to measure the interaction forces between this cellular probe and target surfaces or cells. Initially described for mammalian cells,[96] different protocols have emerged to adapt SCFS to smaller cells, *i.e.* microbes. Tip-less cantilevers are usually coated with poly-L-lysine, Cell-Tak, or polydopamine to attach a single microbial cell at the apex (Fig. 3A).[97,98] Whereas the toxicity of poly-L-Lysine is uncertain, polydopamine—a bio-inspired adhesive—is reported to preserve cell viability.[99-101] However, when probing small cells such as bacteria (~1 µm), the precise positioning of the cell at the apex of the tip-less cantilever is complicated, and unwanted contact between the

tip-less cantilever and the probed surface may occur. In this context, the use of colloidal probes is an attractive alternative, ensuring precise positioning of the bacteria while maintaining its viability.[102] Another elegant technique is fluidic force microscopy (FluidFM) adapted for SCFS of microbial cells which uses hollow cantilevers to apply an under-pressure and trap single cells without the need for chemical fixation, thus allowing the screening of tens to hundreds of cells within hours.[103-105] Although well-suited to yeast cells (Fig. 3B), the application of FluidFM to bacteria remains limited because hollow cantilevers with apertures sufficiently small to immobilize bacteria are not yet commercially available. Nonetheless, focused ion beam milling can be used to mill the aperture of a hollow cantilever to obtain 300–900 nm holes, suitably small to immobilize bacteria.[105] A recent study ingeniously reversed the system, using a commercial hollow cantilever to immobilize a C30-functionalized colloidal silica bead, mimicking the hydrophobic surface of a leaf.[106] This functionalized bead is then used to probe bacterial cells immobilized on a surface at a higher throughput than traditional SCFS methods.

Microbial adhesion revealed by SCFS

Since its development, several studies have demonstrated the importance of the SCFS technique. For instance, *L. rhamnosus* pili interactions with hydrophobic and mucin surfaces produce force signatures indicating nanospring behaviour, whereas those with Caco-2 cells produce force plateaus reflecting membrane tethering.[107] This suggests that the interaction force between pili and Caco-2 cells is not strong enough to induce pili unfolding or that the interaction involves basal regions of the pili (*i.e.* close to the bacterial surface). Similarly, it was demonstrated that type IV pili of *P. aeruginosa* are involved in interactions with both abiotic

surfaces and host pneumocytes.[49] In this case, the force signatures revealed that interactions with abiotic surfaces lead to pili unfolding whereas adhesion to host cells is mediated by both cellular membrane tethers and bacterial pili.

The role of surface adhesins can also be deciphered by SCFS. Analyses of different *P. fluorescens* mutants revealed that LapA promotes adhesion to both hydrophilic and hydrophobic substrates via specific domains of the protein, *i.e.* the C-terminal globular domain for adhesion to hydrophilic substrates and the repeated sequence for hydrophobic interactions.[68] The function and specificity of *Staphylococci* adhesins described at the single-molecule level (see above) were confirmed at the single-cell level by measuring the interactions between individual cells and surfaces coated with different host proteins or chemicals (Fig. 4).[25,72,78,85,86,108] Compared to SMFS, SCFS allows the forces between two living cells to be probed, providing insight into the role of surface adhesins during cell-cell or cell-host interactions. For instance, the cationic PIA was shown to promote *S. aureus* cell-cell adhesion through electrostatic interactions with polyanionic teichoic acids, strengthening the cohesion of the bacterial biofilm.[25] *S. aureus* cellular aggregation is also promoted by the adhesin SasG, and the underlying molecular mechanism was determined by SCFS measurements of the forces between two partner cells (Fig. 4B).[109] This mechanism requires Zn^{2+} to activate cell surface reorganization and unmask SasG proteins from the other cell wall components. Once protruding, SasG promotes cell aggregation through homophilic interactions.[109] This is reminiscent of the roles of SdrC (Fig 4C)[86] and FnBPA,[85] two other surface adhesins in *S. aureus*, for which their role in cell aggregation was demonstrated through homophilic interactions. FnBPA is also implicated in the adhesion of *S. aureus* to host endothelial cells.[84]

Among the bacterial adhesive arsenal, some surface proteins involved in cell-cell adhesion also facilitate bacterial conjugation, or horizontal gene transfer. In the conjugation process, a donor cell comes in contact with a receptor cell, and transfers part of its genetic material, for instance a plasmid. Recently, SCFS has been used to study cell-cell adhesion and the transfer of the pXO16 plasmid in the Gram-positive bacterium *Bacillus thuringiensis*, which is accompanied by macroscopic cellular aggregation.[110] In that study, a donor or receptor cell was immobilized on a colloidal probe, and put in contact with a mating partner long enough for the plasmid to transfer. Their results show that the donor-receptor interaction is very strong and relies on surface proteins encoded by the pXO16 plasmid. In a minimal medium and with enough time for the transconjugant cells to express the plasmid, major changes in the surface adhesive properties were observed. This work demonstrates that SCFS not only allows studying the role of surface proteins at the scale of a single cell-cell pair, but can also be used to induce local gene transfer and study the resulting cell surface changes.

In mixed biofilms, several species interact and SCFS has been used to decipher these interactions. Notably, *S. epidermidis* and *C. albicans* are frequently associated in polymicrobial biofilm infections with enhanced antibiotic resistance. SCFS measurements probing the *C. albicans* surface with single bacterial cells revealed that *S. epidermidis* adhere strongly (~5 nN) on *C. albicans* germ tubes and poorly on yeast cells.[111] This adhesion was attributed to Als and O-mannosylated proteins of the fungal cell wall, as demonstrated with different mutant strains. FluidFM experiments on *C. albicans* cells have recently measured strong Als5-mediated intercellular adhesion with homophilic bonding between Als5 proteins and amyloid-like bond formation (Fig. 3B).[112] In *C. glabrata*, the role of EPA adhesins in adhesion to hydrophobic and hydrophilic abiotic substrates was demonstrated by SCFS.[37,113] The mechanism by which the Flo1 adhesin induces cell aggregation in *S. cerevisiae* was also

demonstrated by measuring interactions between two partner cells:[95] by injecting EDTA or free mannose as blocking agents in the AFM liquid cell during force measurements, they showed that Flo1 adhesion is calcium-dependent and that cell aggregation is governed by the lectin part of the protein, which recognizes mannosides on the partner cell.

In the context of the host-pathogen relationship, SCFS has been used to decipher *C. albicans* interactions with immune cells. It was shown that DC-SIGN receptors on dendritic cells recognize a specific N-mannan structure in the yeast cell wall, and that N-glycans chains of these receptors are essential for the clustering that induces pathogen internalization.[114,115] On macrophages, it was shown that yeast recognition mostly involves mannose receptors, and that *C. albicans*-macrophage interactions lead to the formation of long tethers (up to 100 µm).[116] SCFS has also been used to measure and image the interactions between *S. aureus* and human skin cells.[117-119] The ClfB staphylococcal adhesin has been evidenced as a major actor in such interactions, as it is responsible for mechanically strengthening interactions, notably through the ClfB-loricrin interaction.[81]

Anti-adhesive strategies screened by AFM

Increased bacterial resistance to antibiotics makes blocking bacterial adhesion an attractive alternative to antibiotics in order to prevent bacterial infections linked to biofilm formation. AFM-based force spectroscopy techniques are useful for studying the potential of anti-adhesive strategies and molecules, and several strategies are being pursued to block both non-specific adhesion (*e.g*. hydrophobic interactions) and specific interactions involving different adhesion proteins. In particular, SCFS has been instrumental in deciphering anti-adhesives strategies illustrated through several examples given below.

For example, the capacity of glycofullerenes, as compared to glycomonomers, to block *E. coli* adhesion was quantified and attributed to the enhanced antiadhesive activity of mannofullerene compared to that of heptylmannoside.[63] Similarly, the anti-adhesive effects of charged polymer brushes on *E. coli* were investigated by SCFS, with anionic and neutral brushes leading to decreased *E. coli* adhesion.[120]

Valotteau *et al.* studied the anti-adhesive properties of sophorolipids on the pathogenic bacteria *S. aureus* and *E. coli*.[121] They demonstrated an overall decrease of bacterial adhesion forces and probability on sophorolipid-coated surfaces. Mutant *S. aureus* with no surface adhesins showed further reduced adhesion to the surface, indicating that sophorolipids not only block adhesins, but also other cell wall components such as teichoic acids. The specific targeting of adhesin-ligand interactions has been successful for several staphylococcal adhesins. For instance, a β-neurexin-derived peptide partially blocks SdrC-SdrC interaction (Fig. 4C),[86] and anti-CNA antibodies inhibit the adhesion of *S. aureus* on collagen-coated surfaces.[78]

Anti-adhesion is also being pursued to block the first step of bacterial invasion in the context of host cell-bacteria interactions. The invasion of human lungs by *P. aeruginosa* is facilitated by the interaction of the lectin LecA with the host epithelial cell's globotriaosylceramide.[122] A new therapeutic approach relies on synthetic glycoclusters targeting LecA with higher affinity than its natural ligand. Measurements of the interactions between a human bronchial epithelial cell immobilized on a tip-less AFM cantilever and a bacterial monolayer of *P. aeruginosa* demonstrated promising anti-adhesive properties, with the LecA lectin-glycocluster binding weakening bacteria-cell adhesion.[123]

Perspectives

In addition to traditional AFM imaging, single-cell and single molecule force spectroscopy, new AFM-based approaches have emerged and provide information on microbes and their surface properties. Among them, high-speed AFM has allowed imaging dynamic processes on living cells, helping to decipher, for instance, the mechanism of action of antimicrobial peptides on *E. coli* individual cells in real time.[124,125] Recently, high-speed AFM combined to tapping mode with high-resonance-frequency small and soft cantilevers has also enabled the imaging of intact bacterial photosynthetic organelles with very low applied forces, providing access to single *Rhodobacter sphaeroides* photosystem-protein complexes and intact ATPases.[126] To summarize, high-speed AFM is an increasingly valuable method to characterize microbial envelopes and their proteins in physiologically relevant conditions.

In parallel, AFM has also recently been combined to infrared spectroscopy,[127,128] leading to an exciting method of chemical characterization and mapping with a spatial resolution of ~20-30 nm. Applied to microorganisms, AFM-IR has so far allowed the chemical mapping of intra-cellular nanogranules of polyhydroxybutyrate in *Rhodobacter capsulatus*,[129] and of triacylglycerol in *Streptomyces* bacteria, *Yarrowia* yeast, and *Parachlorella Kessleri* microalgae.[128] Rapid progress has been reported with this technique, leading to label free mapping of thin phospholipid membranes,[130] access to molecular orientation[131] or light-induced conformational changes of bacteriorhodopsin in native purple membrane patches.[132] If so far, AFM-IR is limited to dried samples, it has the potential to become a great tool to better understand the structure and organization of membranes and bacterial envelopes, as well as their interactions with their environment.

Conclusions

The various AFM-based techniques developed in recent years are perfectly suited to deciphering microbial surface properties. AFM imaging has revealed morphological features and cell wall topographical organization in live cells at unprecedented resolution. Single-molecule and single-cell force spectroscopy are powerful tools for unravelling molecular mechanisms by probing the mechanics of individual molecular interactions or the adhesion of entire cells. The dual capability of AFM to probe adhesion at the single-cell and single-molecule scales makes it an attractive tool for the development of anti-adhesive strategies, for which the mode of action must be demonstrated at multiple scales. Indeed, the molecular mechanisms revealed by SMFS can inform the design of new anti-adhesive molecules, and SCFS is suitable for the subsequent screening required to identify the best candidates.

Acknowledgements.

This work was supported by the CNRS MITI interdisciplinary program and the French PIA project “Lorraine Université d’Excellence”, reference ANR-15-IDEX-04-LUE. AB, CF and SEKC are CRCN researchers at the CNRS.

Author contributions.

AB, CF and SEKC wrote the paper.

References

1. L. Hall-Stoodley, J. W. Costerton and P. Stoodley, *Nat Rev Microbiol*, 2004, **2**, 95-108.
2. H. C. Flemming, J. Wingender, U. Szewzyk, P. Steinberg, S. A. Rice and S. Kjelleberg, *Nat Rev Microbiol*, 2016, **14**, 563-575.
3. C. Berne, C. K. Ellison, A. Ducret and Y. V. Brun, *Nat Rev Microbiol*, 2018, **16**, 616-627.
4. A. K. Yadav, A. Espaillat and F. Cava, *Front Microbiol*, 2018, **9**, 2064.
5. A. M. Mitchell and T. J. Silhavy, *Nat Rev Microbiol*, 2019, **17**, 417-428.
6. G. Binnig, C. F. Quate and C. Gerber, *Phys Rev Lett*, 1986, **56**, 930-933.
7. Y. F. Dufrene, D. Martinez-Martin, I. Medalsy, D. Alsteens and D. J. Muller, *Nat Methods*, 2013, **10**, 847-854.
8. D. Alsteens, D. J. Muller and Y. F. Dufrene, *Acc Chem Res*, 2017, **50**, 924-931.
9. Y. F. Dufrene, T. Ando, R. Garcia, D. Alsteens, D. Martinez-Martin, A. Engel, C. Gerber and D. J. Muller, *Nat Nanotechnol*, 2017, **12**, 295-307.
10. A. da Silva, Jr. and O. Teschke, *Biochim Biophys Acta*, 2003, **1643**, 95-103.
11. J. Arfsten, S. Leupold, C. Bradtmoller, I. Kampen and A. Kwade, *Colloids Surf B Biointerfaces*, 2010, **79**, 284-290.
12. A. Jacquot, C. Sakamoto, A. Razafitianamarahavo, C. Caillet, J. Merlin, A. Fahs, J. M. Ghigo, J. F. Duval, C. Beloin and G. Francius, *Nanoscale*, 2014, **6**, 12665-12681.
13. S. Kasas and A. Ikai, *Biophys J*, 1995, **68**, 1678-1680.
14. C. Formosa, F. Pillet, M. Schiavone, R. E. Duval, L. Ressier and E. Dague, *Nat Protoc*, 2015, **10**, 199-204.
15. O. Peric, M. Hannebelle, J. D. Adams and G. E. Fantner, *Nano Research*, 2017, **10**, 3896–3908.
16. V. Dupres, D. Alsteens, K. Pauwels and Y. F. Dufrene, *Langmuir*, 2009, **25**, 9653-9655.
17. T. J. Günther, M. Suhr, J. Raffab and K. Pollmann, *RSC Advances*, 2014, **4**, 51156-51164.
18. G. Francius, S. Lebeer, D. Alsteens, L. Wildling, H. J. Gruber, P. Hols, S. De Keersmaecker, J. Vanderleyden and Y. F. Dufrene, *ACS Nano*, 2008, **2**, 1921-1929.
19. G. Andre, M. Deghorain, P. A. Bron, S. van, II, M. Kleerebezem, P. Hols and Y. F. Dufrene, *ACS Chem Biol*, 2011, **6**, 366-376.
20. E. J. Hayhurst, L. Kailas, J. K. Hobbs and S. J. Foster, *Proc Natl Acad Sci U S A*, 2008, **105**, 14603-14608.
21. G. Andre, S. Kulakauskas, M. P. Chapot-Chartier, B. Navet, M. Deghorain, E. Bernard, P. Hols and Y. F. Dufrene, *Nat Commun*, 2010, **1**, 27.
22. K. Li, X. X. Yuan, H. M. Sun, L. S. Zhao, R. Tang, Z. H. Chen, Q. L. Qin, X. L. Chen, Y. Z. Zhang and H. N. Su, *Front Microbiol*, 2018, **9**, 620.
23. R. S. Dover, A. Bitler, E. Shimoni, P. Trieu-Cuot and Y. Shai, *Nat Commun*, 2015, **6**, 7193.
24. R. D. Turner, S. Mesnage, J. K. Hobbs and S. J. Foster, *Nat Commun*, 2018, **9**, 1263.
25. C. Formosa-Dague, C. Feuillie, A. Beaussart, S. Derclaye, S. Kucharikova, I. Lasa, P. Van Dijck and Y. F. Dufrene, *ACS Nano*, 2016, **10**, 3443-3452.
26. H. A. Eskandarian, P. D. Odermatt, J. X. Y. Ven, M. T. M. Hannebelle, A. P. Nievergelt, N. Dhar, J. D. McKinney and G. E. Fantner, *Nat Microbiol*, 2017, **2**, 17094.
27. R. Boudjemaaa, K. Steenkeste, A. Canette, R. Briandet, M. P. Fontaine-Aupart and C. Marlière, *The Cell Surface*, 2019, **5**, 1-9.

28. E. V. Dubrovin, A. G. Voloshin, S. V. Kraevsky, T. E. Ignatyuk, S. S. Abramchuk, I. V. Yaminsky and S. G. Ignatov, *Langmuir*, 2008, **24**, 13068-13074.
29. D. Alsteens, H. Trabelsi, P. Soumillion and Y. F. Dufrene, *Nat Commun*, 2013, **4**, 2926.
30. B. Hanif, N. Jamil and M. R. Shah, *Springerplus*, 2016, **5**, 2112.
31. G. Francius, O. Domenech, M. P. Mingeot-Leclercq and Y. F. Dufrene, *J Bacteriol*, 2008, **190**, 7904-7909.
32. C. Formosa, M. Grare, R. E. Duval and E. Dague, *Nanomedicine*, 2012, **8**, 12-16.
33. C. Formosa, M. Herold, C. Vidaillac, R. E. Duval and E. Dague, *J Antimicrob Chemother*, 2015, **70**, 2261-2270.
34. D. Alsteens, V. Dupres, K. Mc Evoy, L. Wildling, H. J. Gruber and Y. F. Dufrene, *Nanotechnology*, 2008, **19**, 384005.
35. E. Dague, R. Bitar, H. Ranchon, F. Durand, H. M. Yken and J. M. Francois, *Yeast*, 2010, **27**, 673-684.
36. S. El-Kirat-Chatel, A. Beaussart, D. Alsteens, A. Sarazin, T. Jouault and Y. F. Dufrene, *Nanoscale*, 2013, **5**, 4855-4863.
37. S. El-Kirat-Chatel, A. Beaussart, S. Derclaye, D. Alsteens, S. Kucharikova, P. Van Dijck and Y. F. Dufrene, *ACS Nano*, 2015, **9**, 1648-1655.
38. A. Beaussart, D. Alsteens, S. El-Kirat-Chatel, P. N. Lipke, S. Kucharikova, P. Van Dijck and Y. F. Dufrene, *ACS Nano*, 2012, **6**, 10950-10964.
39. S. El-Kirat-Chatel and Y. F. Dufrene, *ACS Nano*, 2012, **6**, 10792-10799.
40. F. Pillet, S. Lemonier, M. Schiavone, C. Formosa, H. Martin-Yken, J. M. Francois and E. Dague, *BMC Biol*, 2014, **12**, 6.
41. K. S. Kim, Y. S. Kim, I. Han, M. H. Kim, M. H. Jung and H. K. Park, *PLoS One*, 2011, **6**, e28176.
42. S. El-Kirat-Chatel, A. Beaussart, D. Alsteens, D. N. Jackson, P. N. Lipke and Y. F. Dufrene, *Nanoscale*, 2013, **5**, 1105-1115.
43. C. Formosa, M. Schiavone, H. Martin-Yken, J. M. Francois, R. E. Duval and E. Dague, *Antimicrob Agents Chemother*, 2013, **57**, 3498-3506.
44. F. Quiles, I. Accoceberry, C. Couzigou, G. Francius, T. Noel and S. El-Kirat-Chatel, *Nanoscale*, 2017, **9**, 13731-13738.
45. C. Diaz, P. L. Schilardi, R. C. Salvarezza and M. Fernandez Lorenzo de Mele, *Colloids Surf B Biointerfaces*, 2011, **82**, 536-542.
46. G. Francius, P. Polyakov, J. Merlin, Y. Abe, J. M. Ghigo, C. Merlin, C. Beloin and J. F. Duval, *PLoS One*, 2011, **6**, e20066.
47. A. Gillis, V. Dupres, G. Delestrait, J. Mahillon and Y. F. Dufrene, *Nanoscale*, 2012, **4**, 1585-1591.
48. A. Gillis, V. Dupres, J. Mahillon and Y. F. Dufrene, *Micron*, 2012, **43**, 1304-1311.
49. A. Beaussart, A. E. Baker, S. L. Kuchma, S. El-Kirat-Chatel, G. A. O'Toole and Y. F. Dufrene, *ACS Nano*, 2014, **8**, 10723-10733.
50. K. Jonas, H. Tomenius, A. Kader, S. Normark, U. Romling, L. M. Belova and O. Melefors, *BMC Microbiol*, 2007, **7**, 70.
51. J. Rheinlaender, A. Grabner, L. Ott, A. Burkovski and T. E. Schaffer, *Eur Biophys J*, 2012, **41**, 561-570.
52. A. Touhami, M. H. Jericho, J. M. Boyd and T. J. Beveridge, *J Bacteriol*, 2006, **188**, 370-377.
53. P. Tripathi, V. Dupres, A. Beaussart, S. Lebeer, I. J. Claes, J. Vanderleyden and Y. F. Dufrene, *Langmuir*, 2012, **28**, 2211-2216.
54. J. Guerin, J. Burgain, G. Francius, S. El-Kirat-Chatel, A. Beaussart, J. Scher and C. Gaiani, *Food Hydrocoll*, 2018, **82**, 296-303.

55. J. Guerin, C. Soligot, J. Burgain, M. Huguet, G. Francius, S. El-Kirat-Chatel, F. Gomand, S. Lebeer, Y. Le Roux, F. Borges, J. Scher and C. Gaiani, *Colloids Surf B Biointerfaces*, 2018, **167**, 44-53.
56. P. Tripathi, A. Beaussart, D. Alsteens, V. Dupres, I. Claes, I. von Ossowski, W. M. de Vos, A. Palva, S. Lebeer, J. Vanderleyden and Y. F. Dufrene, *ACS Nano*, 2013, **7**, 3685-3697.
57. J. Alegre-Cebollada, C. L. Badilla and J. M. Fernandez, *J Biol Chem*, 2010, **285**, 11235-11242.
58. D. J. Echelman, A. Q. Lee and J. M. Fernandez, *J Biol Chem*, 2017, **292**, 8988-8997.
59. D. J. Echelman, J. Alegre-Cebollada, C. L. Badilla, C. Chang, H. Ton-That and J. M. Fernandez, *Proc Natl Acad Sci U S A*, 2016, **113**, 2490-2495.
60. T. D. Becke, S. Ness, R. Gurster, A. F. Schilling, A. M. di Guilmi, S. Sudhop, M. Hilleringmann and H. Clausen-Schaumann, *ACS Nano*, 2018, **12**, 549-558.
61. T. D. Becke, S. Ness, B. K. Kaufmann, B. Hartmann, A. F. Schilling, S. Sudhop, M. Hilleringmann and H. Clausen-Schaumann, *ACS Nano*, 2019, **13**, 7155-7165.
62. M. Forero, O. Yakovenko, E. V. Sokurenko, W. E. Thomas and V. Vogel, *PLoS Biol*, 2006, **4**, e298.
63. A. Beaussart, M. Abellan-Flos, S. El-Kirat-Chatel, S. P. Vincent and Y. F. Dufrene, *Nano Lett*, 2016, **16**, 1299-1307.
64. A. Alonso-Caballero, J. Schonfelder, S. Poly, F. Corsetti, D. De Sancho, E. Artacho and R. Perez-Jimenez, *Nat Commun*, 2018, **9**, 2758.
65. V. Dupres, F. D. Menozzi, C. Locht, B. H. Clare, N. L. Abbott, S. Cuenot, C. Bompard, D. Raze and Y. F. Dufrene, *Nat Methods*, 2005, **2**, 515-520.
66. L. Arnal, G. Longo, P. Stupar, M. F. Castez, N. Cattelan, R. C. Salvarezza, O. M. Yantorno, S. Kasas and M. E. Vela, *Nanoscale*, 2015, **7**, 17563-17572.
67. R. D. Monds, P. D. Newell, R. H. Gross and G. A. O'Toole, *Mol Microbiol*, 2007, **63**, 656-679.
68. S. El-Kirat-Chatel, A. Beaussart, C. D. Boyd, G. A. O'Toole and Y. F. Dufrene, *ACS Chem Biol*, 2014, **9**, 485-494.
69. R. D. Monds, P. D. Newell, J. C. Wagner, J. A. Schwartzman, W. Lu, J. D. Rabinowitz and G. A. O'Toole, *J Bacteriol*, 2010, **192**, 3011-3023.
70. S. El-Kirat-Chatel, C. D. Boyd, G. A. O'Toole and Y. F. Dufrene, *ACS Nano*, 2014, **8**, 1690-1698.
71. T. J. Foster, J. A. Geoghegan, V. K. Ganesh and M. Hook, *Nat Rev Microbiol*, 2014, **12**, 49-62.
72. P. Herman, S. El-Kirat-Chatel, A. Beaussart, J. A. Geoghegan, T. J. Foster and Y. F. Dufrene, *Mol Microbiol*, 2014, **93**, 356-368.
73. O. Hartford, L. O'Brien, K. Schofield, J. Wells and T. J. Foster, *Microbiology*, 2001, **147**, 2545-2552.
74. P. Herman, S. El-Kirat-Chatel, A. Beaussart, J. A. Geoghegan, T. Vanzieleghem, T. J. Foster, P. Hols, J. Mahillon and Y. F. Dufrene, *Langmuir*, 2013, **29**, 13018-13022.
75. M. Grandbois, M. Beyer, M. Rief, H. Clausen-Schaumann and H. E. Gaub, *Science*, 1999, **283**, 1727-1730.
76. K. Ponnuraj, M. G. Bowden, S. Davis, S. Gurusiddappa, D. Moore, D. Choe, Y. Xu, M. Hook and S. V. Narayana, *Cell*, 2003, **115**, 217-228.
77. L. F. Milles, K. Schulten, H. E. Gaub and R. C. Bernardi, *Science*, 2018, **359**, 1527-1533.
78. P. Herman-Bausier, C. Valotteau, G. Pietrocola, S. Rindi, D. Alsteens, T. J. Foster, P. Speziale and Y. F. Dufrene, *mBio*, 2016, **7**.

79. C. Valotteau, V. Prystopiuk, G. Pietrocola, S. Rindi, D. Peterle, V. De Filippis, T. J. Foster, P. Speziale and Y. F. Dufrene, *ACS Nano*, 2017, **11**, 2160-2170.
80. P. Herman-Bausier, C. Labate, A. M. Towell, S. Derclaye, J. A. Geoghegan and Y. F. Dufrene, *Proc Natl Acad Sci U S A*, 2018, **115**, 5564-5569.
81. P. Vitry, C. Valotteau, C. Feuillie, S. Bernard, D. Alsteens, J. A. Geoghegan and Y. F. Dufrene, *mBio*, 2017, **8**.
82. F. Viela, V. Prystopiuk, A. Leprince, J. Mahillon, P. Speziale, G. Pietrocola and Y. F. Dufrene, *mBio*, 2019, **10**.
83. P. Herman-Bausier, G. Pietrocola, T. J. Foster, P. Speziale and Y. F. Dufrene, *mBio*, 2017, **8**.
84. V. Prystopiuk, C. Feuillie, P. Herman-Bausier, F. Viela, D. Alsteens, G. Pietrocola, P. Speziale and Y. F. Dufrene, *ACS Nano*, 2018, **12**, 3609-3622.
85. P. Herman-Bausier, S. El-Kirat-Chatel, T. J. Foster, J. A. Geoghegan and Y. F. Dufrene, *mBio*, 2015, **6**, e00413-00415.
86. C. Feuillie, C. Formosa-Dague, L. M. Hays, O. Vervaeck, S. Derclaye, M. P. Brennan, T. J. Foster, J. A. Geoghegan and Y. F. Dufrene, *Proc Natl Acad Sci U S A*, 2017, **114**, 3738-3743.
87. V. Dupres, D. Alsteens, S. Wilk, B. Hansen, J. J. Heinisch and Y. F. Dufrene, *Nat Chem Biol*, 2009, **5**, 857-862.
88. V. Dupres, Y. F. Dufrene and J. J. Heinisch, *ACS Nano*, 2010, **4**, 5498-5504.
89. L. L. Hoyer and E. Cota, *Front Microbiol*, 2016, **7**, 280.
90. D. Alsteens, M. C. Garcia, P. N. Lipke and Y. F. Dufrene, *Proc Natl Acad Sci U S A*, 2010, **107**, 20744-20749.
91. D. Alsteens, V. Dupres, S. A. Klotz, N. K. Gaur, P. N. Lipke and Y. F. Dufrene, *ACS Nano*, 2009, **3**, 1677-1682.
92. D. Alsteens, C. B. Ramsook, P. N. Lipke and Y. F. Dufrene, *ACS Nano*, 2012, **6**, 7703-7711.
93. C. Formosa, M. Schiavone, A. Boisrame, M. L. Richard, R. E. Duval and E. Dague, *Nanomedicine*, 2015, **11**, 57-65.
94. B. P. Cormack, N. Ghori and S. Falkow, *Science*, 1999, **285**, 578-582.
95. S. El-Kirat-Chatel, A. Beaussart, S. P. Vincent, M. Abellan Flos, P. Hols, P. N. Lipke and Y. F. Dufrene, *Nanoscale*, 2015, **7**, 1760-1767.
96. J. Helenius, C. P. Heisenberg, H. E. Gaub and D. J. Muller, *J Cell Sci*, 2008, **121**, 1785-1791.
97. N. Thewes, P. Loskill, C. Spengler, S. Humbert, M. Bischoff and K. Jacobs, *Eur Phys J E Soft Matter*, 2015, **38**, 140.
98. G. Zeng, T. Muller and R. L. Meyer, *Langmuir*, 2014, **30**, 4019-4025.
99. H. Lee, S. M. Dellatore, W. M. Miller and P. B. Messersmith, *Science*, 2007, **318**, 426-430.
100. D. Alsteens, A. Beaussart, S. Derclaye, S. El-Kirat-Chatel, H. R. Park, P. N. Lipke and Y. F. Dufrene, *Anal Methods*, 2013, **5**, 3657-3662.
101. A. Beaussart, S. El-Kirat-Chatel, P. Herman, D. Alsteens, J. Mahillon, P. Hols and Y. F. Dufrene, *Biophys J*, 2013, **104**, 1886-1892.
102. A. Beaussart, S. El-Kirat-Chatel, R. M. Sullan, D. Alsteens, P. Herman, S. Derclaye and Y. F. Dufrene, *Nat Protoc*, 2014, **9**, 1049-1055.
103. A. Meister, M. Gabi, P. Behr, P. Studer, J. Voros, P. Niedermann, J. Bitterli, J. Polesel-Maris, M. Liley, H. Heinzelmann and T. Zambelli, *Nano Lett*, 2009, **9**, 2501-2507.
104. E. Potthoff, O. Guillaume-Gentil, D. Ossola, J. Polesel-Maris, S. LeibundGut-Landmann, T. Zambelli and J. A. Vorholt, *PLoS One*, 2012, **7**, e52712.

105. E. Potthoff, D. Ossola, T. Zambelli and J. A. Vorholt, *Nanoscale*, 2015, **7**, 4070-4079.
106. M. Mittelviefhaus, D. B. Muller, T. Zambelli and J. A. Vorholt, *ISME J*, 2019, **13**, 1878-1882.
107. R. M. Sullan, A. Beaussart, P. Tripathi, S. Derclaye, S. El-Kirat-Chatel, J. K. Li, Y. J. Schneider, J. Vanderleyden, S. Lebeer and Y. F. Dufrene, *Nanoscale*, 2014, **6**, 1134-1143.
108. E. Maikranz, C. Spengler, N. Thewes, A. Thewes, F. Nolle, P. Jung, M. Bischoff, L. Santen and K. Jacobs, *Nanoscale*, 2020, DOI: 10.1039/d0nr03134h.
109. C. Formosa-Dague, P. Speziale, T. J. Foster, J. A. Geoghegan and Y. F. Dufrene, *Proc Natl Acad Sci U S A*, 2016, **113**, 410-415.
110. C. Feuillie, C. Valotteau, L. Makart, A. Gillis, J. Mahillon and Y. F. Dufrene, *Nano Lett*, 2018, **18**, 5821-5826.
111. A. Beaussart, P. Herman, S. El-Kirat-Chatel, P. N. Lipke, S. Kucharikova, P. Van Dijck and Y. F. Dufrene, *Nanoscale*, 2013, **5**, 10894-10900.
112. J. Dehullu, C. Valotteau, P. Herman-Bausier, M. Garcia-Sherman, M. Mittelviefhaus, J. A. Vorholt, P. N. Lipke and Y. F. Dufrene, *Nano Lett*, 2019, **19**, 3846-3853.
113. C. Valotteau, V. Prystopiuk, B. P. Cormack and Y. F. Dufrene, *mSphere*, 2019, **4**.
114. J. Te Riet, B. Joosten, I. Reinieren-Beeren, C. G. Figdor and A. Cambi, *Sci Rep*, 2017, **7**, 6713.
115. J. Te Riet, I. Reinieren-Beeren, C. G. Figdor and A. Cambi, *J Mol Recognit*, 2015, **28**, 687-698.
116. S. El-Kirat-Chatel and Y. F. Dufrene, *Nanoscale Horiz*, 2016, **1**, 69-74.
117. C. Formosa-Dague, Z. H. Fu, C. Feuillie, S. Derclaye, T. J. Foster, J. A. Geoghegan and Y. F. Dufrene, *Nanoscale Horiz*, 2016, **1**, 298-303.
118. O. M. Fleury, M. A. McAleer, C. Feuillie, C. Formosa-Dague, E. Sansevere, D. E. Bennett, A. M. Towell, W. H. I. McLean, S. Kezic, D. A. Robinson, P. G. Fallon, T. J. Foster, Y. F. Dufrene, A. D. Irvine and J. A. Geoghegan, *Infect Immun*, 2017, **85**.
119. C. Feuillie, P. Vitry, M. A. McAleer, S. Kezic, A. D. Irvine, J. A. Geoghegan and Y. F. Dufrene, *mBio*, 2018, **9**.
120. Y. J. Oh, E. S. Khan, A. D. Campo, P. Hinterdorfer and B. Li, *ACS Appl Mater Interfaces*, 2019, **11**, 29312-29319.
121. C. Valotteau, N. Baccile, V. Humblot, S. Roelants, W. Soetaert, C. V. Stevens and Y. F. Dufrêne, *Nanoscale Horizons*, 2019, **4**, 975-982.
122. T. Eierhoff, B. Bastian, R. Thuenauer, J. Madl, A. Audfray, S. Aigal, S. Juillot, G. E. Rydell, S. Muller, S. de Bentzmann, A. Imberty, C. Fleck and W. Romer, *Proc Natl Acad Sci U S A*, 2014, **111**, 12895-12900.
123. F. Zuttion, C. Ligeour, O. Vidal, M. Walte, F. Morvan, S. Vidal, J. J. Vasseur, Y. Chevolot, M. Phaner-Goutorbe and H. Schillers, *Nanoscale*, 2018, **10**, 12771-12778.
124. G. E. Fantner, R. J. Barbero, D. S. Gray and A. M. Belcher, *Nat Nanotechnol*, 2010, **5**, 280-285.
125. C. Formosa-Dague, R. E. Duval and E. Dague, *Semin Cell Dev Biol*, 2018, **73**, 165-176.
126. S. Kumar, M. L. Cartron, N. Mullin, P. Qian, G. J. Leggett, C. N. Hunter and J. K. Hobbs, *ACS Nano*, 2017, **11**, 126-133.
127. A. Dazzi, F. Glotin and R. Carminati, *J Appl Phys*, 2010, **107**, 124519-124526.
128. A. Dazzi and C. B. Prater, *Chem Rev*, 2017, **117**, 5146-5173.
129. C. Mayet, A. Dazzi, R. Prazeres, J. M. Ortega and D. Jaillard, *Analyst*, 2010, **135**, 2540-2545.

130. B. Kastner, C. M. Johnson, P. Hermann, M. Kruskopf, K. Pierz, A. Hoehl, A. Hornemann, G. Ulrich, J. Fehmel, P. Patoka, E. Ruhl and G. Ulm, *ACS Omega*, 2018, **3**, 4141-4147.
131. E. Lipiec, A. Wnetrzak, A. Chachaj-Brekiesz, W. Kwiatek and P. Dynarowicz-Latka, *J Colloid Interface Sci*, 2019, **542**, 347-354.
132. V. Giliberti, R. Polito, E. Ritter, M. Broser, P. Hegemann, L. Puskar, U. Schade, L. Zanetti-Polzi, I. Daidone, S. Corni, F. Rusconi, P. Biagioni, L. Baldassarre and M. Ortolani, *Nano Lett*, 2019, **19**, 3104-3114.

Figure legends

Figure 1. High resolution AFM imaging reveals bacterial S-layer and peptidoglycan structures. A) AFM images of side-wall peptidoglycan from *Bacillus subtilis* at different growth phases. Scales bars = 200 nm (a-d) and 100 nm (e,f). (B) AFM images of *Escherichia coli* peptidoglycan organization (left) together with gradient organisation map (right) indicating the tendency of the structure to order. Scales bars = 50 nm (C-D) Images of *Viridibacillus arvi* (C, D bottom) and *Lysinibacillus sphaericus* (D, top) depicting S-layer envelopes. (E) S-layer is visible at the surface of *Corynebacterium glutamicum* grown in specific growth medium.
(A) has been reproduced from ref[22]. (B) has been reproduced from ref[24], with permission from Springer Nature. (C-D) have been reproduced from ref[17], with permission from RSC Publishing. (E) has been reproduced from ref[16], with permission from the American Chemical Society.

Figure 2. Single-molecule force spectroscopy allows to decipher adhesion and nanomechanics of bacterial appendages. A) Primary structure of the subunits constituting pili of the Gram-positive bacteria *Lactobacillus rhamnosus* GG. B) AFM image of *Lactobacillus rhamnosus* GG living bacteria trapped in a porous membrane, with pili structures imaged in air depicted in the inset (left). Pulling single pili with pilin-subunits-decorated tips (right) results in various force-distance curves profiles. C) Representative force-distance curves of pili unfolding revealing single adhesion force peaks with linear, spring-like shapes and characteristic steps; red numbers correspond to linear segments of increasing slopes. Such patterns helped to understand the nanomechanical response of pili under external force. D) Primary structure of LapA, an adhesin from the Gram-negative bacteria *Pseudomonas fluorescens*. E) AFM image *of Pseudomonas fluorescens* living bacteria trapped in a porous membrane (left). AFM tips functionalized with anti-HA antibodies were used to detect HA-

779 tagged LapA molecules at the surface of living cells. F) Representative force-distance curves
780 of LapA protein unfolding. The sawtooth patterns observed on the curve correspond to the
781 sequential unfolding of repeated patterns in the protein sequence. Red lines correspond to
782 worm-like-chain model fit.
783 (A-C) have been modified from ref[56], with permission from the American Chemical Society. (D-
784 F) have been reproduced from ref[68], with permission from the American Chemical Society.
785

786 **Figure 3. Methodologies used to attach a single-cell to the AFM cantilever.** (A) Single-cell
787 force spectroscopy consists in approaching a biological-glue (polydopamine) coated tip-less
788 cantilever towards a living cell (here yeast) to attach it to the cantilever and then probe its
789 adhesion on different (bio)-surfaces. (B) With the FluidFM set-up, a single cell is immobilized
790 on the cantilever aperture by applying a negative pressure. The cell probe is then moved
791 toward a target cell immobilized in a porous membrane and force-distance curves are
792 recorded.
793 (A) has been reproduced from ref[100], with permission from the Royal Society of Chemistry. (B)
794 has been reproduced from ref[112], with permission from the American Chemical Society.
795

796 **Figure 4. Deciphering the binding mechanism of different *Staphylococcal* adhesins by single-**
797 **cell force spectroscopy**. SCFS with *Staphylococcus* bacteria used as a bioprobe revealed that
798 (A) its adhesin SdrG binds to fibrinogen following a 'dock, lock and latch' model with strong
799 forces of ~ 2 nN; (B) Zinc activates the adhesive function of the adhesin SasG in homophilic
800 cell-cell interactions with representative sawtooth patterns specific of SasG protein unfolding
801 and (C) the adhesin SdrC is engaged in low affinity intercellular adhesion below 500 pN and
802 strong cellular interactions with hydrophobic surfaces.

803 (A) has been modified from ref[72], with permission from John Wiley and Sons, (B) from ref[109]

804 and (C) from ref[86], with permission from the National Academy of Science.

805

806 **Figure 1**

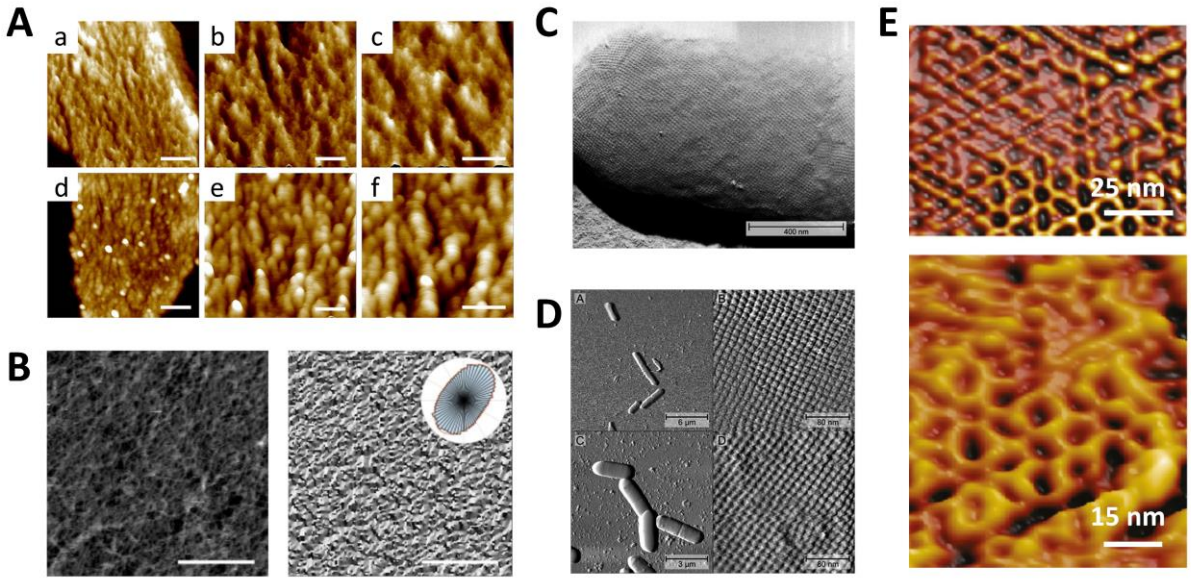

807

808

809 **Figure 2**

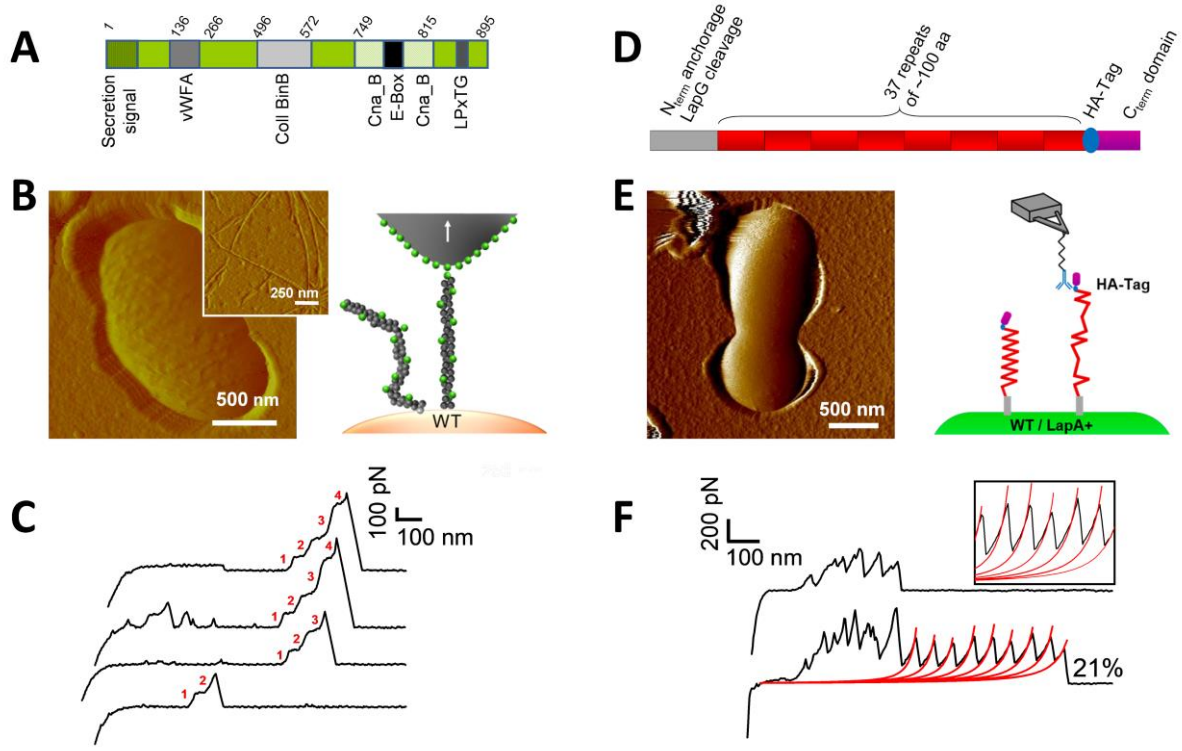

810

811

812 **Figure 3**

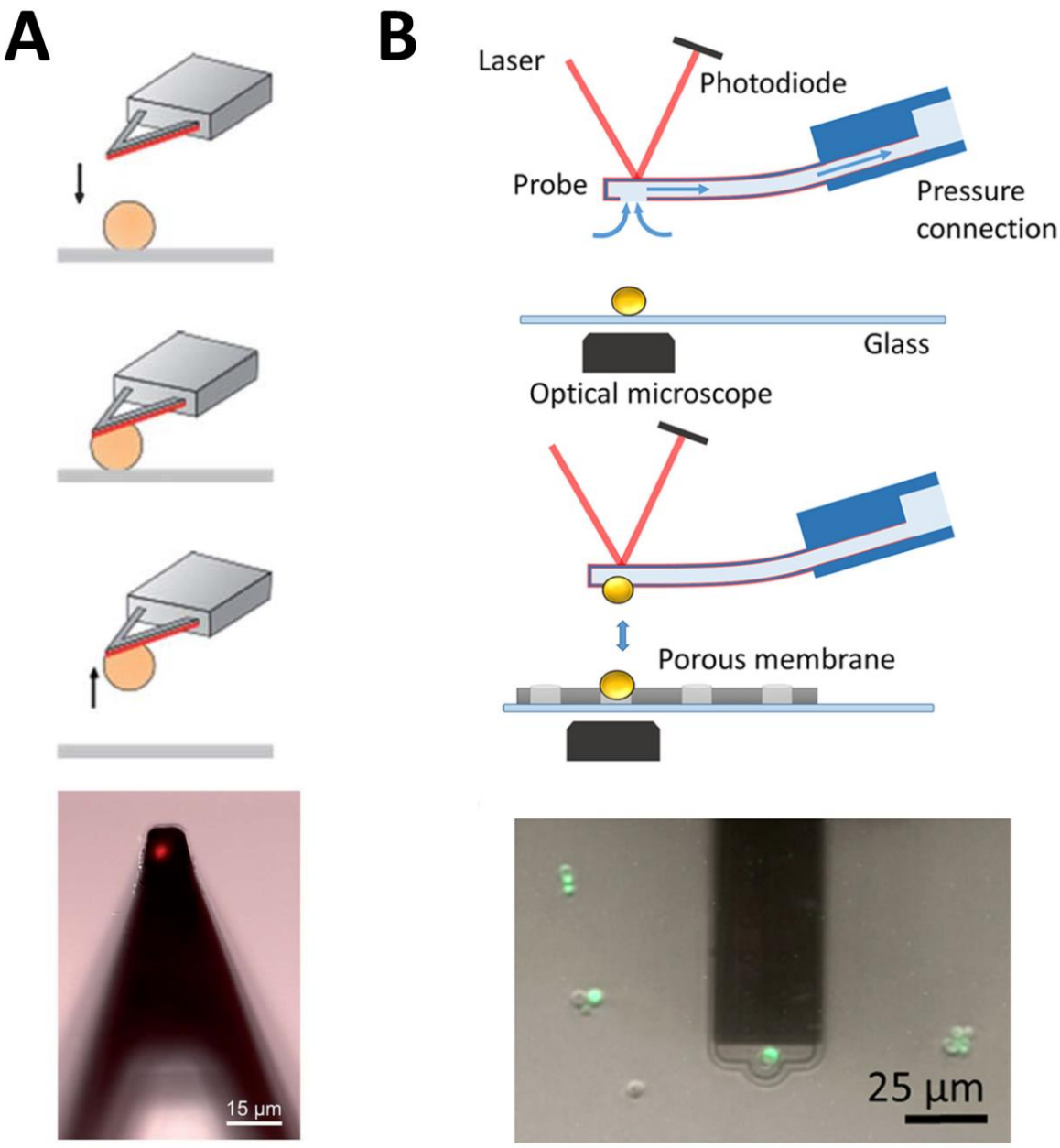

813

814

815 **Figure 4**

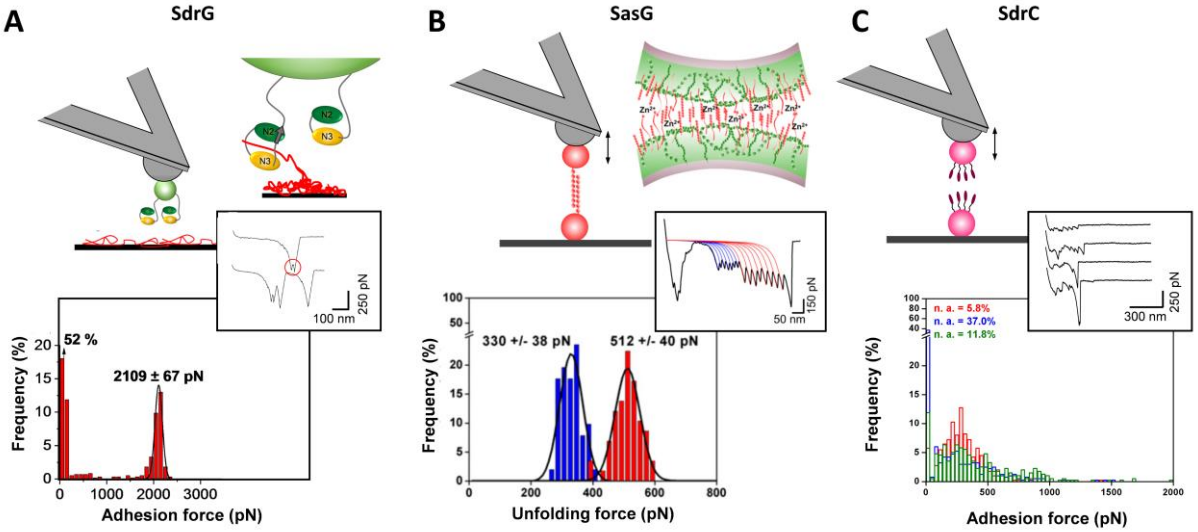

816

817